frontiers in Earth Science

ORIGINAL RESEARCH
published: 25 November 2021
doi: 10.3389/feart.2021.761748

Geochemical and Mineralogical Characteristics of Garnierite From the Morowali Ni-Laterite Deposit in Sulawesi, Indonesia

Yuri Choi[1], *Insung Lee*[1]* *and Inkyeong Moon*[2]

[1]School of Earth and Environmental Sciences, Seoul National University, Seoul, South Korea, [2]Deep-Sea and Seabed Mineral Resources Research Center, Korea Institute of Ocean Science and Technology, Busan, South Korea

The Morowali Ni-laterite deposit is located in the East Sulawesi Ophiolite, which is a large ophiolite belt on Sulawesi Island, Indonesia. The Morowali deposit is developed on a laterite profile due to ophiolite weathering, with saprolite, limonite, and ferruginous cap horizons from the bottom to top. Based on the occurrence of garnierite as the main ore, occurring in the saprolite horizon, it can be classified that the ore deposit is hydrous Mg silicate-type. The Ni ore is classified into different types based on color and XRD and electron probe micro-analyzer analyses. Whole-rock geochemical study was also conducted to understand the mineralization process. The Morowali Ni deposit consists of serpentine-like and talc-like phases. The serpentine-like phase consists of Ni-lizardite and karpinskite (0.76–38.26 wt% NiO) while the talc-like phase is mainly composed of kerolite (4.02–8.02 wt% NiO). The serpentine-like garnierite exhibits high Ni and Fe contents and occurrence similar to that of the serpentine observed in the saprolite horizon, suggesting the serpentine-like garnierite originated from the bedrock, and Mg-Ni cation exchange occurred during laterization. Contrastingly, the lower Fe content of the talc-like phase (0.01–0.05 wt%) than the serpentine-like phase (0.14–7.03 wt%) indicates that the talc-like garnierite is of secondary origin since Fe is immobile during weathering. The Morowali Ni-laterite deposit was mainly formed during laterization. The repetition of dry and wet cycles in each year results in the formation of secondary garnierite.

Keywords: Morowali Ni-laterite deposit, garnierite, Mg-Ni hydrous silicate, ophiolite laterization, Indonesia

OPEN ACCESS

Edited by:
Sean C. Johnson,
University College Dublin, Ireland

Reviewed by:
Mohd Basril Iswadi Basori,
National University of Malaysia, Malaysia
Kit Lai,
Universiti Brunei Darussalam, Brunei

***Correspondence:**
Insung Lee
insung@snu.ac.kr

Specialty section:
This article was submitted to Economic Geology, a section of the journal Frontiers in Earth Science

Received: *20 August 2021*
Accepted: *03 November 2021*
Published: *25 November 2021*

Citation:
Choi Y, Lee I and Moon I (2021) Geochemical and Mineralogical Characteristics of Garnierite From the Morowali Ni-Laterite Deposit in Sulawesi, Indonesia. Front. Earth Sci. 9:761748. doi: 10.3389/feart.2021.761748

INTRODUCTION

Nickel is an important metal that is used to manufacture stainless steel, metal alloys, and rechargeable batteries. Therefore, its demand and production have been constantly increasing since the 20th century (Mudd, 2010; Mudd and Jowitt, 2014). Nickel ores are produced in both magmatic sulfide and laterite-type deposits. The magmatic sulfide deposits occur within the deep crust and are generated by a high degree of partial melting of the mantle that contains Ni-rich sulfide liquids (Barnes and Lightfoot, 2005), while Ni-bearing laterite deposits are developed by the weathering of ultramafic rocks under humid conditions such as tropical or sub-tropical climates (Butt and Cluzel, 2013; Butt, 2016). Although laterite-type Ni deposits account for 60% of the global nickel resources, ~60% of the world nickel production is dependent on sulfide-type ores owing to their convenience in processing (Elias, 2002; Dalvi et al., 2004; Mudd, 2010; Butt and Cluzel, 2013; Mudd and Jowitt,

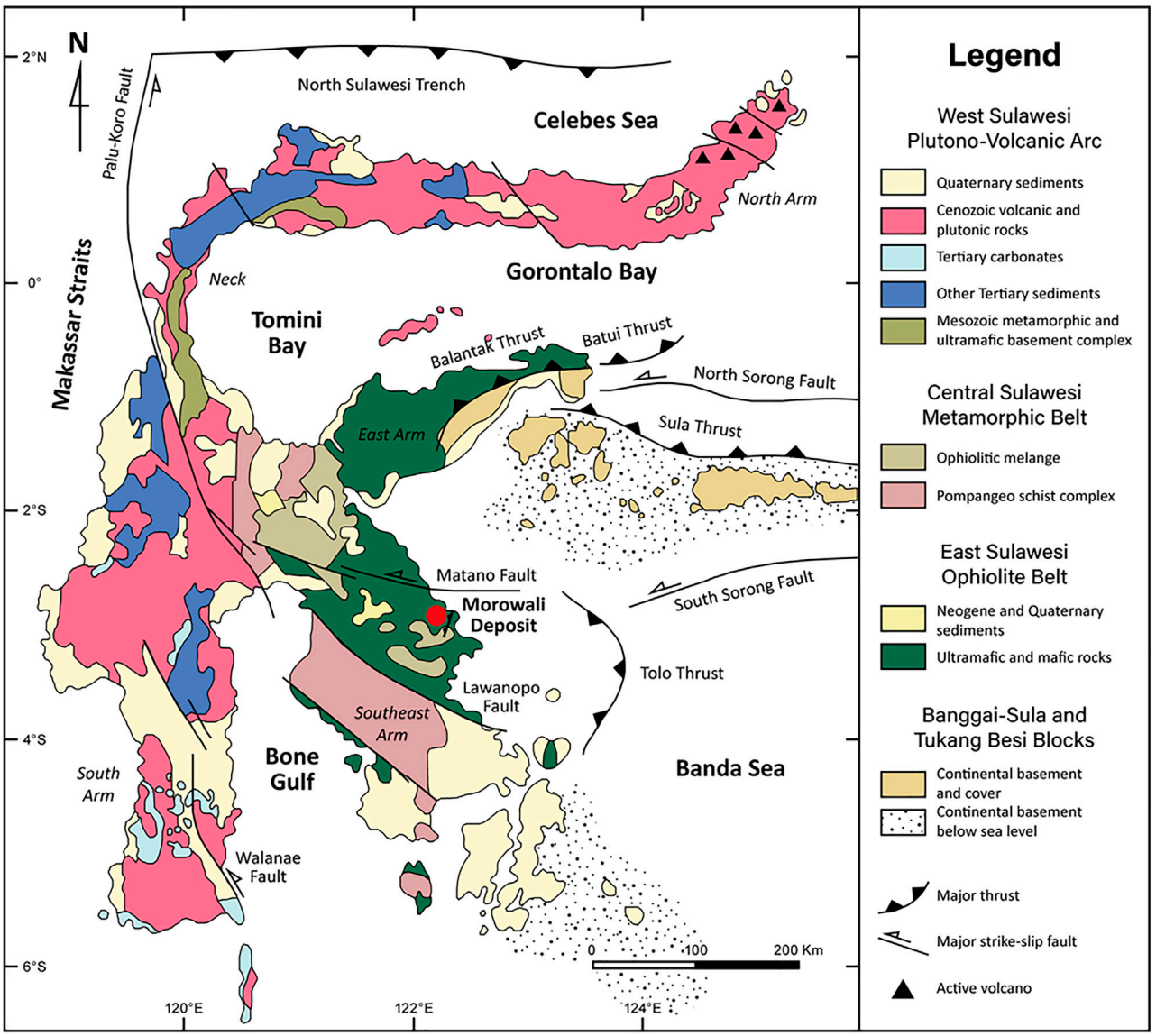

FIGURE 1 | Geological map of Sulawesi island, Indonesia and location of Morowali deposit (modified after Hall and Wilson (2000)). The location of the Morowali deposit is shown in the red circle.

2014). It is believed that there will be a rise in the demand for Ni; lateritic Ni deposits have recently gained attention since they can be utilized to meet this demand.

Lateritic Ni deposits can be classified into three types according to their dominant Ni-bearing mineral groups, i.e., oxide (Fe oxyhydroxides), hydrous Mg-silicate (Ni-rich hydrous silicates), and clay silicate (Ni-rich smectites) deposits (Golightly, 1979; Freyssinet et al., 2005; Butt and Cluzel, 2013). Most laterite-type Ni deposits are distributed in countries that lie within 22°N and S latitudes, such as the Philippines, Indonesia, New Caledonia, Brazil, Dominican Republic, Colombia, and Venezuela (Elias, 2002; Butt and Cluzel, 2013). The Ni-rich hydrous Mg-silicates are the representative Ni ores in the hydrous Mg-silicate deposits and are generally referred to informally as garnierite. Garnierite is a yellowish green to bluish green colored aphanitic mineral containing high Ni concentration, up to 19.9% (Brand, 1998). Although there is still debate on the classification of garnierite because of its origins, it is known that garnierite is a mixture of various hydrous silicates. It is divided into two groups depending on the silicate layer type: 1:1 and 2:1, which are the ratios between tetrahedral and octahedral sheet in hydrous silicates (Brindley and Hang, 1973; Brindley, 1980). The first layer group consists of serpentine minerals, such as lizardite–népouite, chrysotile–pecoraite, and berthierine–brindleyite series; the second layer comprises talc–willemseite, kerolite–pimelite, clinochlore–nimite, and sepiolite–falcondoite series (Brindley, 1980). The most common natural associations for the hydrous

Mg-Ni silicates are with lizardite–nepouite and kerolite–pimelite series (Brindley, 1980). These mineral series are generally referred to as serpentine-like (7 Å-type) garnierite (1:1 group) and talc-like (10 Å-type) garnierite (2:1 group) (Brindley and Hang, 1973; Freyssinet et al., 2005; Butt and Cluzel, 2013; Villanova-de-Benavent et al., 2014; Fu et al., 2018).

In this study, we investigated the Ni-rich laterite deposits in Morowali, Sulawesi, Indonesia to understand garnierite genesis and mineralization during laterization based on mineralogical and geochemical studies. Also, we suggest genetic model of the Morowali Ni laterite deposit.

GEOLOGICAL SETTING

Regional Geological Setting

Sulawesi Island has a complex tectonic setting, which is a result of the collision between the Eurasian, Indian-Australian, and Pacific plates during the Late Cretaceous and Early Tertiary (Katili, 1978; Wilson and Moss, 1999; Hall and Wilson, 2000; Kadarusman et al., 2004). Consequently, the K-shaped Sulawesi island is surrounded by thrusts and has four distinct litho-tectonic belts from west to east: 1) West Sulawesi plutono-volcanic arc, 2) Central Sulawesi metamorphic belt, 3) East Sulawesi ophiolite, and 4) microcontinental blocks of Banggai-Sula and Buton-Tukang Besi (Hall and Wilson, 2000). The study area, Morowali deposit, is located in the East Sulawesi ophiolite belt (**Figure 1**).

According to the tectonic reconstructions of Southeast Asia, the Sulawesi ophiolite was accreted onto the Eurasian plate during subduction of the Indian-Australian plate in the Late Oligocene (Hall, 1997; Parkinson, 1998). The East Sulawesi ophiolite is considered as one of the largest ophiolites in the world, covering more than 15,000 km^2 with a total length of 700 km (Monnier et al., 1995; Kadarusman et al., 2004; Van der Ent et al., 2013). The East Sulawesi ophiolite comprises two lithological units: 1) Neogene and Quaternary sediments; 2) ultramafic and mafic rocks (**Figure 1**). The ophiolite belt is 70% peridotites, composed of lherzolite, harzburgite, and occasional dunite (Kadarusman et al., 2004). The Morowali area principally consists of harzburgite and lherzolite; however, these peridotites are highly altered to serpentinite, making it difficult to identify their original mineral composition and texture. The ophiolitic mélange zone belonging to the Central Sulawesi metamorphic belt is also exposed near the study area along with the active and earthquake-inducing Matano fault (Stevens et al., 1999).

The bedrock lithology, tectonic setting, age of weathering with respect to tectonic activity, climate, and topography control Ni-rich laterite formation (Freyssinet et al., 2005). The Morowali area has a tropical rainforest climate with annual average temperature of 27°C and 2,000 mm of annual precipitation, which makes the area thickly forested with a diverse vegetation in accordance with the elevation. The study area has a moderate relief and gentle slope. Furthermore, the well-developed drainage system of the bedrock promotes Ni-rich laterite profiles in a large area and aids in the formation of high-grade Mg-silicate minerals.

Nickel Laterite Deposit Geology and Sample Description

Geological Characteristics of Ni Laterite Deposit

The Morowali Ni-laterite deposit is located in the southeast arm of the East Sulawesi Ophiolite Belt (**Figure 1**). The Ni-rich laterite profile of the Morowali deposit is developed on top of the bedrock and distinguished into three horizons, from bottom to top: saprolite, limonite, and ferruginous cap (**Figure 2A**). These horizons are classified according to their dominant color, mineralogy, fractures, and texture. The laterite profile of the study area has highly variable thicknesses, ranging 8–19 m, because of the undulatory boundaries of each horizon (**Figures 2A,B**). The part from the top of the saprolite horizon to the ferruginous cap has mostly become soil, making the original form of the top horizon hard to distinguish.

Garnierite usually occurs in the lower saprolite horizon as a coating over the ultramafic rocks with a remarkably distinguishable jade green to grass green color (**Figures 2E–H**). It is aphanitic and fine-grained, showing different shades of green and/or white to yellowish colored grains (**Figures 2H–J**). In addition, some aphanitic garnierite occurs as veins, along the joints. Both the coatings and veins are <1 mm thick. The mineralogical characteristics of each horizon are as follows:

Bedrock

The bedrock in the Morowali area mainly comprises harzburgite and lherzolite (**Figures 2C,D**), usually consisting of serpentine and orthopyroxene as the major phases with minor fine-grained olivine and iddingsite. Although the peridotites in the study area undergo weathering and serpentinization, orthopyroxene occurs as the dominant mineral. The orthopyroxenes are subhedral to euhedral, 1–3 mm in diameter, with exsolution lamellae of clinopyroxene (**Figures 3A,B**). Serpentine occurs as a secondary alteration mineral along joints or cleavages, surrounding or infiltrating the orthopyroxene grains (**Figure 3A**) and/or shows a mesh texture (**Figures 3C,H**). The more weathered orthopyroxenes were altered to clay that occurred as a coating on the orthopyroxene grains (**Figure 3B**). Only a few fine-grained olivines are visible due to their alteration mainly into serpentine with minor iddingsite, which is a reddish- or yellowish-brown colored amorphous mineral (**Figure 3C**).

Saprolite

The saprolite horizon changes color, from yellowish-brown, grayish-yellow, or grayish-green, with respect to the degree of weathering. The thickness of the horizon is 2–7 m, and it is the main ore body in the study area. Most of the horizon consists of fine-grained earthy saprolite and coarse rocky saprolite. The coarse rock fragments partially preserve the original texture of the bedrock. Discontinuous stockwork are developed and garnierite veins or coatings precipitate along this stockwork. Alteration products such as fibrous serpentinite, talc, and clay are also accompanied by the stockwork.

Under microscopic observation, the rocky saprolite has a texture similar to that of the bedrock, but with comparatively more serpentine. The difference between the bedrock and the

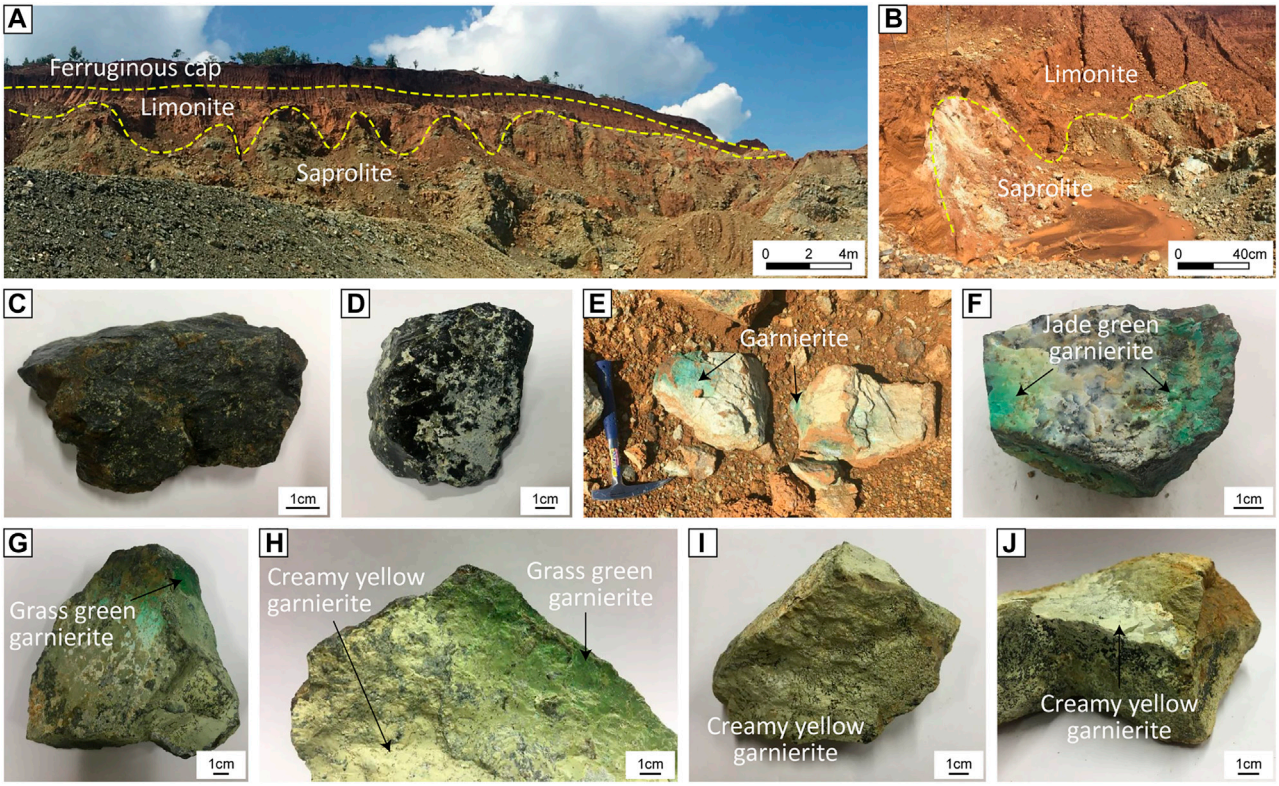

FIGURE 2 | Photographs of lateritic horizons in the Morowali deposit and representative samples from each horizon. Laterite profile **(A)** and undulatory boundary between limonite and saprolite horizon **(B)**. Rock samples from bottom to top **(C)** and **(D)** bedrock **(E)**–**(J)** garnierite samples distinguished by its colors.

saprolite is the presence of mesh-textured serpentine in the saprolite with more secondary minerals such as clay minerals and chromite (**Figures 3C–H**). Serpentine is the most abundant mineral in the saprolite horizon and coexists with orthopyroxene, which is preserved in the bedrock. Almost all the serpentine grains have a tarnished brown or greenish brown color with a mesh texture. A minor form of serpentine was also observed cross-cutting the mesh serpentine and orthopyroxene (**Figures 3D,H**). This serpentine appears as a micro-veinlet and resembles the last stage of serpentine mineralization during weathering. The chrome oxides of <1.2 mm size are surrounded by serpentine and occur as anhedral grains (**Figure 3H**).

Both grass green (**Figure 3E**) and jade green colored (**Figure 3F**) garnierites occur as coatings and show aphanitic character in the macroscopic observation. The grass green colored garnierite contains a dark green Mg-silicate without any remarkable texture, while the jade green colored garnierite contains an ivory colored Mg-silicate with oscillational texture. At the edge of the saprolite and the grass-green garnierite, a ~150 μm thick silicate rim was observed. The vein-type garnierite has a mélange green color in plane-polarized light (**Figure 3G**). Iddingsite and magnetite developed in the vein-type garnierite during its formation.

Limonite

The limonite horizon is a reddish-brown soil consisting of clay minerals. It is 2–7 m thick with a undulating boundary between limonite and saprolite at some places. Two distinct zones are recognized in the limonite horizon, the lower yellow limonite and upper red limonite. Both are composed of goethite and hematite, which make the soil reddish-brown in color due to iron oxidation. However, goethite is the main mineral constituent in the yellow limonite zone, while hematite is the main constituent of the red limonite zone. The original texture of the bedrock is not visible because of the intense weathering in this horizon.

Ferruginous Cap

The ferruginous cap is the top horizon of the Ni-rich laterite profile, which only occurs in the highland area. It is a dark reddish-brown duricrust, rich in ferrous minerals such as hematite. The ferruginous cap is relatively thinner than the lower horizons (1–2 m) (**Figure 2A**). The boundary between the ferruginous cap and the limonite horizon shows a clear distinction. The ferruginous cap could not be observed on the inclined exposures due to erosion (**Figure 2A**).

ANALYTICAL METHODS

Thirteen samples were collected from the bedrock and each of the laterite layers except for the ferruginous cap (Three from bedrock, nine saprolite, and one from limonite) and analyzed by X-ray diffraction (XRD) and X-ray fluorescence spectrometry (XRF) at the National Center for Inter-University Research Facility (NCIRF), Seoul National

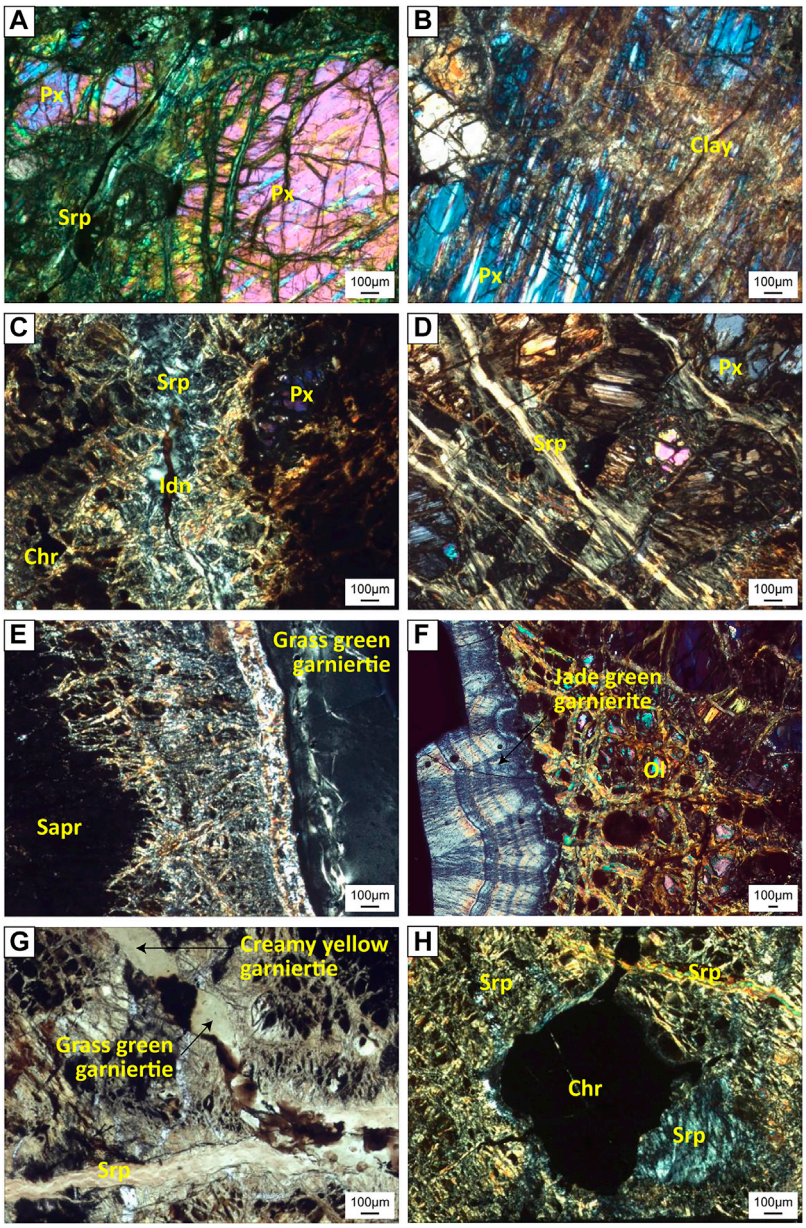

FIGURE 3 | Photomicrographs of the Morowali deposit samples. All photomicrographs except **(G)** were taken under cross-polarized light (XPL). **(A)** phenocrysts of orthopyroxene surrounded by serpentine **(B)** altered orthopyroxene with clinopyroxene exsolutions **(C)** serpentine and development of iddingsite **(D)** serpentine vein crosscutting the bedrock **(E)** and **(F)** development of grass green and jade green garnierite **(G)** veins of serpentine and creamy yellow garnierite **(H)** anhedral chromite phenocryst surrounded by serpentine. Abbreviation: Px = pyroxene, Srp = serpentine, Idn = iddingsite, Chr = chromite, Sapr = saprolite.

University. Mineral chemical analysis was conducted using electron probe micro-analyzer (EPMA) at the Center for Research Facility, Gyeongsang National University and NCIRF, and scanning electron microscopy and energy dispersive spectroscopy (SEM-EDS) was conducted at the School of Earth and Environmental Sciences, Seoul National University.

XRD Analysis

Before the powder XRD analysis, three different colors of garnierite (creamy yellow, grass green, and jade green) were separated from the saprolite samples by handpicking. Each sample was ground into the size of 200 mesh in an agate mortar. XRD analysis was carried out on the garnierite samples using the Rigaku SmartLab with 2θ angles from 5°to 80°, step size of 0.02°, and step duration of 2°s. The mineral phases were indexed using PDXL software and PDF-2 database.

EPMA and SEM Analyses

Six thin sections from the bedrock and saprolite horizon were prepared for EPMA and SEM analyses. Quantitative mineral

TABLE 1 | Summary of the garnierite characteristics from this study.

Sample	Classification	Color	XRD	Structural formula	NiO content from EPMA (wt%)
S1-2, S3-1	Serpentine-like	creamy yellow	7 Å	$(Mg_{2.22\text{-}2.63}Ni_{0.03\text{-}0.33}Fe_{0.17\text{-}0.26})Si_{2.05\text{-}2.14}O_5(OH)_4$	0.76–8.41
S1-2, S1-3, S2-2		grass green	7 + 10 Å	$(Mg_{0.53\text{-}2.65}Ni_{0.03\text{-}1.63}Fe_{0.01\text{-}0.30})Si_{2.02\text{-}2.41}O_5(OH)_4$	0.76–38.26
G-1, G-3	Talc-like	jade green	10 Å	$(Mg_{2.64\text{-}2.80}Ni_{0.22\text{-}0.44})Si_{3.94\text{-}3.99}O_{10}(OH)_2{\cdot}nH_2O$	4.02–8.02

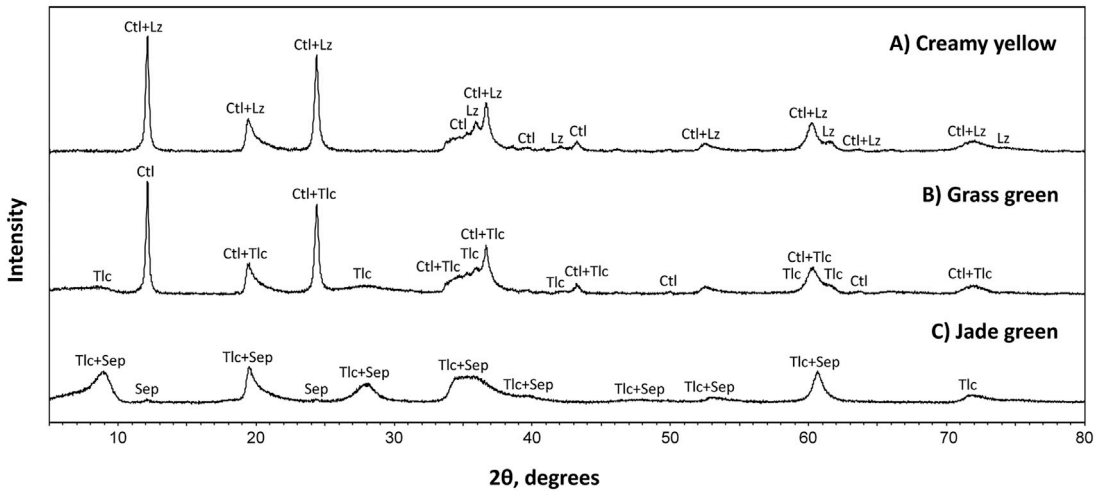

FIGURE 4 | XRD patterns of three garnierite samples from the Morowali deposit distinguished by their colors. Unlike the jade green sample, both the creamy yellow and grass green samples show similar patterns. However, the grass green sample has a mixed pattern between creamy yellow and jade green samples. Abbreviation: Lz = lizardite, Ctl = chrysotile, Tlc = talc, Sep = sepiolite.

analyses were performed using field emission EPMA (JEOL JXA-8530F) and field emission SEM (JEOL JSM-7100F). The field emission EPMA is equipped with five WDS channels and one EDS channel. The applied accelerating voltage was 15 kV, the probe current was 20 nA, and the beam size was 3 μm. Calibration was performed using natural and synthetic standard materials: jadeite (Na), albite (Si), fayalite (Fe), K-feldspar (K), wollastonite (Ca), MgO (Mg), Al_2O_3 (Al), MnO (Mn), TiO_2 (Ti), Cr_2O_3 (Cr), and NiO (Ni). The field emission SEM had an accelerating voltage 15 kV, working distance of 10 mm and an emission current of 53 nA.

XRF Analysis

Twelve samples from the bedrock (B-2, B-3, and G-2), saprolite (G-1, G-3, S1-1, S1-2, S2-1, S2-2, S3-1, and S3-2), and limonite horizon (L-1) were powdered into 200 mesh in an agate mortar for whole rock analysis. Major (SiO_2, Al_2O_3, TiO_2, Fe_2O_3, MgO, CaO, Na_2O, K_2O, MnO, and P_2O_5) and trace elements (NiO and Cr_2O_3), and SO_3 were determined using Shimadzu XRF-1700. Loss on ignition (LOI), which is the weight loss of the sample after burning at 950°C was also measured. Samples were analyzed using lithium tetraborate ($Li_2B_4O_7$) glass beads. The determination limit was better than 10 ppm, and the analytical uncertainties are less than ±2%.

RESULTS

Mineralogical Characteristics of Garnierite

Table 1 summarizes the characteristics of garnierites and their structural formulae. According to XRD and EPMA analyses, garnierite of the Morowali deposit can be distinguished into serpentine- and talc-like. The serpentine-like garnierite occurs in creamy yellow and grass green varieties. XRD pattern of the creamy yellow garnierite (S1-2 and S3-1) shows chrysotile and lizardite phases (**Figure 4A**). The creamy yellow garnierite contains 42.17–44.26 wt% of SiO_2, 30.88–36.83 wt% of MgO, 4.14–6.43 wt% of FeO, and 0.76–8.41 wt% of NiO (**Table 2**). The concentrations of TiO_2, Al_2O_3, Cr_2O_3, MnO, Co, CaO, Na_2O, and K_2O were <0.1 wt%. The general chemical formula of serpentine-like garnierite is $(Mg,Ni)_3Si_2O_5(OH)_4$ (Brindley, 1980; Brand, 1998; Freyssinet et al., 2005), and its structural formulae was calculated using seven oxygens (Brindley and Hang, 1973). Each element concentration is represented in atoms per formula unit (apfu) in **Table 2**. Elements under 0.01 apfu were considered as negligible for the structural formulae calculation. The calculated structural formula for the creamy yellow garnierite is $(Mg_{2.22\text{-}2.63}Ni_{0.03\text{-}0.33}Fe_{0.17\text{-}0.26})Si_{2.05\text{-}2.14}O_5(OH)_4$.

The grass green garnierite (S1-2, S1-3, and S2-2) exhibited mixed XRD patterns with serpentine-like and talc-like structures (**Figure 4B**). The grass green garnierite is composed of

TABLE 2 | EPMA data of serpentine- and talc-like garnierites (in wt%).

Garnierite	Serpentine-like garnierite						
Color	Creamy yellow						
Sample	S1-2						
Spot	1	2	21	22	23	24	25
SiO_2	44.26	42.17	42.66	42.90	43.42	42.91	43.82
TiO_2	0.00	0.01	0.02	0.02	0.01	0.00	0.00
$Al2O_3$	0.02	0.03	0.05	0.04	0.02	0.05	0.00
$Cr2O_3$	0.00	0.00	0.01	0.00	0.00	0.03	0.00
FeO	4.14	4.89	6.43	5.53	5.06	5.36	4.67
MgO	30.88	33.37	35.37	36.76	36.78	36.83	35.69
NiO	8.41	4.57	1.35	1.12	0.76	1.19	1.00
MnO	0.03	0.02	0.07	0.07	0.07	0.04	0.06
CoO	0.00	0.10	—	—	—	—	—
CaO	0.04	0.02	0.03	0.03	0.04	0.04	0.05
Na_2O	0.03	0.00	0.02	0.01	0002E03	0.00	0.05
K_2O	0.08	0.08	0.02	0.01	0.02	0.01	0.03
Total	87.88	85.26	86.03	86.49	86.20	86.47	85.37
Oxygen							
Si	2.14	2.08	2.06	2.05	2.07	2.05	2.10
Ti	0.00	0.00	0.00	0.00	0.00	0.00	0.00
Al	0.00	0.00	0.00	0.00	0.00	0.00	0.00
ΣTetr.	2.14	2.08	2.07	2.06	2.07	2.06	2.10
Cr	0.00	0.00	0.00	0.00	0.00	0.00	0.00
Fe	0.17	0.20	0.26	0.22	0.20	0.21	0.19
Mg	2.22	2.45	2.55	2.62	2.62	2.63	2.56
Ni	0.33	0.18	0.05	0.04	0.03	0.05	0.04
Mn	0.00	0.00	0.00	0.00	0.00	0.00	0.00
Co	0.00	0.00	—	—	—	—	—
Ca	0.00	0.00	0.00	0.00	0.00	0.00	0.01
Na	0.00	0.00	0.00	0.00	0.00	0.00	0.00
K	0.00	0.00	0.00	0.00	0.00	0.00	0.00
ΣOct.	2.73	2.84	2.87	2.89	2.86	2.89	2.80
T/O	0.78	0.73	0.72	0.71	0.73	0.71	0.75
Ni/Mg	0.15	0.07	0.02	0.02	0.01	0.02	0.02

Garnierite	Serpentine-like garnierite																					
Color	Grass green																					
Sample	S1-2	S1-3																				
Spot	3	1	2	3	4	5	6	7	8	9	10	11	12	13	14	15	16	17	18	19	20	21
SiO_2	46.69	48.25	42.39	44.98	41.36	41.60	41.23	42.13	43.06	43.67	46.33	46.35	45.77	45.48	45.78	47.77	44.27	46.78	47.12	43.92	48.23	46.95
TiO_2	0.00	0.02	0.03	0.00	0.00	0.02	0.01	0.00	0.00	0.02	0.00	0.00	0.00	0.00	0.01	0.00	0.01	0.00	0.00	0.01	0.02	0.01
$Al2O_3$	0.00	0.02	0.05	0.00	0.01	0.03	0.02	0.02	0.04	0.02	0.01	0.01	0.00	0.00	0.02	0.01	0.03	0.00	0.02	0.02	0.01	0.02
$Cr2O_3$	0.01	0.03	0.00	0.00	0.00	0.00	0.00	0.00	0.00	0.00	0.00	0.00	0.00	0.00	0.00	0.01	0.00	0.01	0.01	0.00	0.00	0.00
FeO	2.31	2.08	5.67	0.46	6.33	6.30	7.03	5.12	5.48	4.71	0.18	0.25	0.24	0.14	3.47	1.82	3.65	1.08	1.98	3.93	1.40	2.09
MgO	22.06	24.51	36.68	9.08	35.78	27.48	28.45	35.53	37.39	29.68	10.39	7.44	7.19	6.70	25.51	21.92	29.35	19.32	23.40	29.93	20.41	23.68
NiO	16.12	16.65	1.39	35.13	2.22	9.88	8.57	2.72	0.76	8.72	35.83	37.92	37.92	38.26	14.08	17.72	9.65	19.11	16.12	9.18	19.88	16.28
MnO	0.00	0.00	0.03	0.10	0.04	0.02	0.02	0.04	0.04	0.01	0.02	0.06	0.09	0.03	0.03	0.02	0.03	0.02	0.00	0.05	0.02	0.00

(Continued on following page)

TABLE 2 | (*Continued*) EPMA data of serpentine- and talc-like garnierites (in wt%).

Garnierite	Serpentine-like garnierite																					
Color	Grass green																					
Sample	S1-2	S1-3																				
Spot	3	1	2	3	4	5	6	7	8	9	10	11	12	13	14	15	16	17	18	19	20	21
CoO	0.00	0.00	—	—	—	—	—	—	—	—	—	—	—	—	—	—	—	—	—	—	—	—
CaO	0.05	0.08	0.01	0.05	0.01	0.04	0.07	0.05	0.01	0.04	0.08	0.08	0.06	0.09	0.05	0.05	0.03	0.08	0.05	0.03	0.06	0.06
Na_2O	0.00	0.02	0.02	0.05	0.00	0.02	0.03	0.00	0.01	0.03	0.02	0.01	0.03	0.00	0.03	0.03	0.04	0.02	0.02	0.03	0.03	0.04
K_2O	0.18	0.13	0.02	0.08	0.03	0.08	0.04	0.01	0.00	0.05	0.06	0.04	0.06	0.05	0.07	0.08	0.05	0.11	0.08	0.04	0.09	0.05
Total	87.42	91.79	86.28	89.93	85.80	85.47	85.46	85.61	86.80	86.94	92.90	92.16	91.35	90.75	89.05	89.43	87.11	86.53	88.80	87.14	90.15	89.18
Oxygen																						
Si	2.31	2.28	2.04	2.38	2.02	2.12	2.09	2.05	2.05	2.14	2.36	2.41	2.41	2.41	2.23	2.32	2.16	2.36	2.29	2.15	2.34	2.28
Ti	0.00	0.00	0.00	0.00	0.00	0.00	0.00	0.00	0.00	0.00	0.00	0.00	0.00	0.00	0.00	0.00	0.00	0.00	0.00	0.00	0.00	0.00
Al	0.00	0.00	0.00	0.00	0.00	0.00	0.00	0.00	0.00	0.00	0.00	0.00	0.00	0.00	0.00	0.00	0.00	0.00	0.00	0.00	0.00	0.00
ΣTetr.	2.31	2.28	2.04	2.38	2.02	2.12	2.10	2.05	2.05	2.14	2.36	2.41	2.41	2.41	2.23	2.32	2.16	2.36	2.29	2.15	2.34	2.28
Cr	0.00	0.00	0.00	0.00	0.00	0.00	0.00	0.00	0.00	0.00	0.00	0.00	0.00	0.00	0.00	0.00	0.00	0.00	0.00	0.00	0.00	0.00
Fe	0.10	0.08	0.23	0.02	0.26	0.27	0.30	0.21	0.22	0.19	0.01	0.01	0.01	0.01	0.14	0.07	0.15	0.05	0.08	0.16	0.06	0.08
Mg	1.63	1.72	2.63	0.72	2.61	2.08	2.15	2.58	2.65	2.17	0.79	0.58	0.56	0.53	1.85	1.59	2.14	1.45	1.70	2.18	1.48	1.71
Ni	0.64	0.63	0.05	1.49	0.09	0.40	0.35	0.11	0.03	0.34	1.47	1.59	1.60	1.63	0.55	0.69	0.38	0.78	0.63	0.36	0.78	0.64
Mn	0.00	0.00	0.00	0.00	0.00	0.00	0.00	0.00	0.00	0.00	0.00	0.00	0.00	0.00	0.00	0.00	0.00	0.00	0.00	0.00	0.00	0.00
Co	0.00	0.00	—	—	—	—	—	—	—	—	—	—	—	—	—	—	—	—	—	—	—	—
Ca	0.01	0.01	0.00	0.01	0.00	0.00	0.01	0.00	0.00	0.00	0.01	0.01	0.01	0.01	0.01	0.00	0.00	0.01	0.01	0.00	0.01	0.01
Na	0.00	0.00	0.00	0.00	0.00	0.00	0.00	0.00	0.00	0.00	0.00	0.00	0.00	0.00	0.00	0.00	0.00	0.00	0.00	0.00	0.00	0.00
K	0.01	0.01	0.00	0.01	0.00	0.01	0.00	0.00	0.00	0.00	0.00	0.00	0.00	0.00	0.00	0.00	0.00	0.01	0.00	0.00	0.01	0.00
ΣOct.	2.38	2.46	2.92	2.25	2.96	2.77	2.82	2.90	2.90	2.72	2.28	2.19	2.19	2.18	2.55	2.37	2.68	2.29	2.42	2.71	2.32	2.45
T/O	0.97	0.93	0.70	1.06	0.68	0.77	0.74	0.71	0.71	0.79	1.04	1.10	1.10	1.11	0.87	0.98	0.81	1.03	0.95	0.79	1.01	0.93
Ni/Mg	0.39	0.37	0.02	2.09	0.03	0.19	0.16	0.04	0.01	0.16	1.86	2.75	2.85	3.08	0.30	0.44	0.18	0.53	0.37	0.17	0.53	0.37

Garnierite	Talc-like garnierite														
Color	Jade green														
Sample	G1-1														
Spot	1	2	3	4	5	6	7	8	9	10	11	12	13	14	15
SiO_2	56.76	56.96	58.98	58.38	58.10	58.30	57.86	58.88	59.38	58.34	58.32	57.55	59.42	59.26	58.22
TiO_2	0.01	0.01	0.00	0.01	0.00	0.01	0.01	0.00	0.00	0.00	0.00	0.02	0.01	0.02	0.01
Al_2O_3	0.00	0.y00	0.00	0.00	0.00	0.00	0.01	0.00	0.00	0.00	0.00	0.00	0.00	0.00	0.01
Cr_2O_3	0.03	0.00	0.00	0.00	0.00	0.01	0.00	0.01	0.00	0.00	0.00	0.00	0.00	0.03	0.00
FeO	0.05	0.01	0.01	0.01	0.00	0.01	0.02	0.02	0.00	0.01	0.03	0.00	0.02	0.00	0.01
MgO	26.27	26.74	26.44	27.19	25.99	25.99	25.91	26.30	27.09	26.09	26.17	26.09	27.61	27.93	27.63
NiO	6.87	4.75	6.66	5.32	7.84	7.57	7.98	6.68	5.60	7.58	7.19	8.02	4.67	4.02	4.86
MnO	0.02	0.00	0.03	0.00	0.02	0.04	0.01	0.02	0.03	0.02	0.01	0.01	0.02	0.05	0.02
CoO	0.00	0.00	—	—	—	—	—	—	—	—	—	—	—	—	—
CaO	0.03	0.04	0.03	0.03	0.02	0.02	0.02	0.03	0.04	0.03	0.02	0.02	0.02	0.03	0.02
Na_2O	0.06	0.01	0.00	0.03	0.02	0.01	0.02	0.01	0.04	0.00	0.00	0.01	0.00	0.01	0.02
K_2O	0.05	0.07	0.06	0.09	0.05	0.03	0.03	0.04	0.10	0.04	0.04	0.04	0.05	0.07	0.04
Total	90.15	88.58	92.21	91.06	92.05	92.00	91.88	92.00	92.28	92.11	91.79	91.77	91.81	91.42	90.85
Oxygen															
Si	3.94	3.97	3.98	3.97	3.96	3.97	3.96	3.99	3.99	3.97	3.97	3.94	3.99	3.98	3.96
Ti	0.00	0.00	0.00	0.00	0.00	0.00	0.00	0.00	0.00	0.00	0.00	0.00	0.00	0.00	0.00

(Continued on following page)

TABLE 2 | (*Continued*) EPMA data of serpentine- and talc-like garnierites (in wt%).

Garnierite	Talc-like garnierite														
Color	Jade green														
Sample	G1-1														
Spot	1	2	3	4	5	6	7	8	9	10	11	12	13	14	15
Al	0.00	0.00	0.00	0.00	0.00	0.00	0.00	0.00	0.00	0.00	0.00	0.00	0.00	0.00	0.00
ΣTetr	3.94	3.97	3.98	3.97	3.96	3.97	3.96	3.99	3.99	3.97	3.97	3.94	3.99	3.99	3.96
Cr	0.00	0.00	0.00	0.00	0.00	0.00	0.00	0.00	0.00	0.00	0.00	0.00	0.00	0.00	0.00
Fe	0.00	0.00	0.00	0.00	0.00	0.00	0.00	0.00	0.00	0.00	0.00	0.00	0.00	0.00	0.00
Mg	2.72	2.78	2.66	2.76	2.64	2.64	2.64	2.65	2.71	2.64	2.66	2.66	2.76	2.80	2.80
Ni	0.38	0.27	0.36	0.29	0.43	0.41	0.44	0.36	0.30	0.41	0.39	0.44	0.25	0.22	0.27
Mn	0.00	0.00	0.00	0.00	0.00	0.00	0.00	0.00	0.00	0.00	0.00	0.00	0.00	0.00	0.00
Co	0.00	0.00	–	–	–	–	–	–	–	–	–	–	–	–	–
Ca	0.00	0.01	0.00	0.00	0.00	0.00	0.00	0.00	0.01	0.00	0.00	0.00	0.00	0.00	0.00
Na	0.01	0.00	0.00	0.00	0.00	0.00	0.00	0.00	0.01	0.00	0.00	0.00	0.00	0.00	0.00
K	0.00	0.01	0.00	0.01	0.00	0.00	0.00	0.00	0.01	0.00	0.00	0.00	0.00	0.01	0.00
ΣOct	3.13	3.06	3.04	3.06	3.08	3.06	3.09	3.03	3.04	3.07	3.06	3.12	3.02	3.03	3.08
T/O	1.26	1.30	1.31	1.30	1.29	1.30	1.28	1.32	1.31	1.29	1.30	1.27	1.32	1.31	1.29
Ni/Mg	0.14	0.10	0.14	0.11	0.16	0.16	0.17	0.14	0.11	0.16	0.15	0.17	0.09	0.08	0.09

41.23–48.25 wt% of SiO_2, 6.70–37.39 wt% of MgO, 0.14–7.03 wt % of FeO, and a higher amount of NiO (0.76–38.26 wt%) than creamy yellow and talc-like garnierites (**Table 2**). The structural formula of grass green garnierite was also calculated in the same way as that of creamy yellow garnierite. The calculated structural formula for grass green garnierite is $(Mg_{0.53\text{-}2.65}Ni_{0.03\text{-}1.63}Fe_{0.01\text{-}0.30})Si_{2.02\text{-}2.41}O_5(OH)_4$.

The talc-like garnierite (G-1 and G-3) exhibited a jade green color, and consists of comparatively higher concentrations of SiO_2 (56.76–59.42 wt%), MgO (25.91–27.93 wt%), and NiO (4.02–8.02 wt%) while the other elements exist in trace amounts (<0.1 wt%) (**Table 2**). The general chemical formula for talc-like garnierite is $(Mg,Ni)_3Si_4O_{10}(OH)_2{\cdot}nH_2O$ (Brindley, 1980; Brand, 1998; Freyssinet et al., 2005). The structural formulae of talc-like garnierite were calculated on the basis of 11 oxygen atoms (Brindley and Hang, 1973). Mg and Ni were allocated to the octahedral site, while Si was allocated to the tetrahedral site. Due to the trace amounts of Ti, Al, Cr, Fe, Mn, Co., Ca, Na, and K (<0.01 apfu), only Si (3.94–3.99 apfu), Mg (2.64–2.80 apfu), and Ni (0.22–0.44 apfu) were considered for calculation of the structural formulae (**Table 2**). The estimated structural formula is $(Mg_{2.64\text{-}2.80}Ni_{0.22\text{-}0.44})Si_{3.94\text{-}3.99}O_{10}(OH)_2{\cdot}nH_2O$.

Geochemical Characteristics of Bedrock and Saprolite Horizon

Pyroxene and serpentine are abundant minerals in the bedrock saprolite horizon with minor occurrence of chromite. The EPMA data for these minerals are presented in **Table 3**. Pyroxenes in the bedrock and saprolite horizon have similar amounts of SiO_2 (51.35–56.88 wt%), MgO (15.86–33.43 wt%), CaO (0.94–23.2 wt %), FeO (2.32–6.13 wt%), and NiO (0.02–0.15 wt%). The wide ranges of MgO and CaO are probably due to clinopyroxene exsolutions in orthopyroxene (**Figures 3A,B**). Serpentines show a narrow range of SiO_2 (40.12–43.35 wt%) in the bedrock and saprolite samples, while MgO and NiO show a wide variation (27.54–37.1 wt% and 0.97–7.84 wt%, respectively). It was also observed that the NiO content was inversely proportional to the MgO content. This variation indicates a high degree of cation exchange between Ni and Mg at this level. Additionally, chromites with variable Al_2O_3, FeO, and MgO contents were also observed. Such chromites were distinguished into high-Al and low-Al chromites. The high-Al chromites contains relatively lower FeO (16.09–17.37 wt%) and higher MgO (13.76–14.88 wt %) than the low-Al chromites (57.39 wt% FeO and 1.05 wt% MgO).

Whole Rock Geochemistry of Laterite Profile

The major and trace elements concentrations in the bedrock and saprolite horizon are generally similar (**Table 4**). SiO_2, MgO, and Fe_2O_3 were the most abundant in the bedrock and saprolite horizon. SiO_2, MgO, and Fe_2O_3 contents for the bedrock and saprolite horizon vary between 38.79–43.91 wt%, 27.65–36.27 wt

TABLE 3 | EPMA data from minerals in the bedrock and saprolite (in wt%).

Sample	Mineral	Spot	Chemical composition											
			SiO_2	TiO_2	Al_2O_3	Cr_2O_3	FeO	MgO	NiO	MnO	CoO	CaO	Na_2O	K_2O	Total
S2-1	Pyroxene	1	56.88	0.02	2.54	0.71	5.81	33.43	0.06	0.18	0.00	0.96	0.00	0.00	100.58
		2	56.06	0.00	2.71	0.80	5.70	33.11	0.07	0.14	0.25	1.04	0.00	0.01	99.89
		3	52.72	0.06	2.98	1.08	2.32	17.28	0.09	0.14	0.00	23.16	0.01	0.01	99.85
	Olivine	1	40.99	0.04	0.00	0.00	8.75	49.81	0.46	0.18	0.07	0.02	0.00	0.00	100.32
	Serpentine	1	41.85	0.00	1.12	0.47	5.89	27.54	7.84	0.11	0.00	0.04	0.04	0.08	84.99
		2	42.82	0.02	1.45	0.41	7.41	28.84	6.14	0.02	0.00	0.05	0.05	0.10	87.32
	Chromite	1	0.00	0.03	32.65	37.00	16.09	14.88	0.19	0.28	0.07	0.00	0.03	0.00	101.22
		2	0.02	0.03	32.77	35.86	16.84	14.46	0.13	0.25	0.00	0.00	0.00	0.00	100.36
S1-3	Pyroxene	1	55.63	0.13	3.01	0.68	6.12	32.90	0.10	0.12	0.07	0.94	0.03	0.00	99.74
	Serpentine	1	43.35	0.01	0.03	0.00	4.14	32.52	6.10	0.03	0.15	0.04	0.00	0.07	86.45
		2	42.48	0.02	0.11	0.00	4.41	36.61	1.44	0.03	0.00	0.03	0.00	0.02	85.14
S1-2	Pyroxene	1	55.81	0.02	2.39	0.72	5.50	31.98	0.11	0.15	0.00	2.72	0.00	0.00	99.39
	Serpentine	1	41.85	0.00	0.00	0.02	5.31	35.93	1.78	0.07	0.01	0.04	0.04	0.06	85.12
		2	42.72	0.00	0.09	0.02	5.25	36.76	1.15	0.06	0.08	0.01	0.03	0.03	86.20
		3	41.63	0.00	0.45	0.00	5.46	30.96	5.95	0.06	0.00	0.04	0.04	0.07	84.65
		4	40.74	0.00	0.10	0.04	7.34	33.90	2.09	0.06	0.02	0.05	0.04	0.08	84.45
	Chromite	1	0.00	0.01	28.23	41.78	16.19	14.64	0.12	0.27	0.00	0.00	0.00	0.01	101.24
		2	0.00	0.06	29.11	39.29	17.01	14.07	0.16	0.23	0.37	0.00	0.00	0.01	100.31
		3	0.00	0.00	4.32	33.99	57.39	1.05	0.17	0.79	0.00	0.00	0.02	0.00	97.74
G1-1	Pyroxene	1	56.34	0.00	2.24	0.76	5.39	32.92	0.12	0.10	0.03	1.75	0.05	0.01	99.70
		2	56.31	0.04	2.52	0.77	5.82	32.88	0.11	0.19	0.00	1.58	0.00	0.00	100.22
		3	55.95	0.06	2.49	0.74	5.54	32.09	0.15	0.07	0.26	2.62	0.00	0.01	99.97
	Serpentine	1	40.95	0.02	0.00	0.05	4.99	37.10	0.97	0.06	0.00	0.01	0.02	0.00	84.16
		2	40.12	0.00	0.00	0.05	6.92	33.75	2.56	0.04	0.01	0.01	0.00	0.04	83.49
		3	42.49	0.00	0.49	0.00	5.93	35.09	1.72	0.06	0.05	0.02	0.01	0.04	85.88
	Chromite	1	0.01	0.00	27.16	42.71	17.32	14.04	0.12	0.20	0.55	0.00	0.00	0.00	102.10
		2	0.03	0.00	26.36	42.00	17.37	13.76	0.21	0.22	0.61	0.00	0.02	0.01	100.58
B-2	Pyroxene	1	56.13	0.11	3.09	0.83	6.13	32.64	0.10	0.13	0.00	1.02	0.00	0.01	100.18
		2	55.25	0.10	3.60	0.81	5.85	31.21	0.08	0.14	0.08	2.71	0.03	0.00	99.84
		3	55.63	0.13	3.01	0.68	6.12	32.90	0.10	0.12	0.07	0.94	0.03	0.00	99.74
		4	51.35	0.26	4.42	1.24	2.85	15.86	0.02	0.08	0.00	23.20	0.33	0.00	99.60

TABLE 4 | XRF data of bedrock, saprolite, and limonite horizon samples (in wt%).

Sample	Bedrock			Saprolite								Limonite
	B-2	B-3	G-2	G-1	G-3	S1-1	S1-2	S2-1	S2-2	S3-1	S3-2	L-1
SiO_2	42.46	43.91	41.50	42.08	41.86	39.43	39.83	40.09	38.79	38.94	39.80	2.59
Al_2O_3	2.32	2.39	2.02	0.83	1.09	0.84	0.75	0.98	0.92	1.00	1.08	5.92
TiO_2	0.04	0.06	0.05	0.01	0.01	0.00	0.00	0.01	0.01	0.00	0.01	0.05
Fe_2O_3*	8.33	8.50	8.38	8.46	7.60	8.02	8.01	8.85	9.20	10.44	10.36	66.90
MgO	36.27	35.28	36.19	31.04	32.66	35.49	33.89	30.19	30.65	27.65	28.76	0.74
CaO	1.89	2.03	1.78	0.64	0.88	0.67	0.59	0.66	0.31	0.74	0.72	0.02
Na_2O	0.21	0.18	0.16	0.11	0.20	0.14	0.16	0.11	0.13	0.12	0.11	0.09
K_2O	0.011	0.02	0.01	0.01	0.008	0.01	0.006	0.01	0.007	0.008	0.01	0.013
MnO	0.13	0.13	0.12	0.12	0.10	0.11	0.10	0.12	0.11	0.12	0.14	1.22
P_2O_5	0.004	0.004	0.004	0.003	0.004	0.006	0.005	0.003	0.005	0.004	0.003	0.003
NiO	0.45	0.46	0.64	3.14	1.03	0.70	1.46	5.14	3.72	4.03	4.66	1.83
Cr_2O_3	0.58	0.66	0.75	0.57	0.52	0.57	0.32	0.63	0.57	0.72	0.70	3.78
SO_3	n.d	0.06	0.05	n.d	n.d	n.d	n.d	n.d	n.d	n.d	n.d	0.72
L.O.I	7.31	6.35	8.37	12.99	14.04	14.03	14.88	13.19	15.60	16.24	13.63	16.14
Total	100.02	100.03	100.02	100.01	99.99	100.01	99.99	99.98	100.01	100.00	99.99	100.03

L.O.I, loss on ignition; Fe_2O_3, total iron oxide; n.d, not detected.*

%, and 7.6–10.44 wt%, respectively. However, those for the limonite horizon exhibited lower SiO_2 (2.59 wt%) and MgO (0.74 wt%), and higher Fe_2O_3 (66.9 wt%) values. The contents of immobile elements, such as Al_2O_3, Cr_2O_3, and MnO, are below 6 wt% in all the horizons. Minor amounts of CaO (1.89–0.02 wt %) and Na_2O (0.21–0.09 wt%) with extremely low K_2O and P_2O_5 (<0.01%) were also observed. NiO (0.45–5.14 wt%) is abundant in saprolite horizon and depleted in the bedrock.

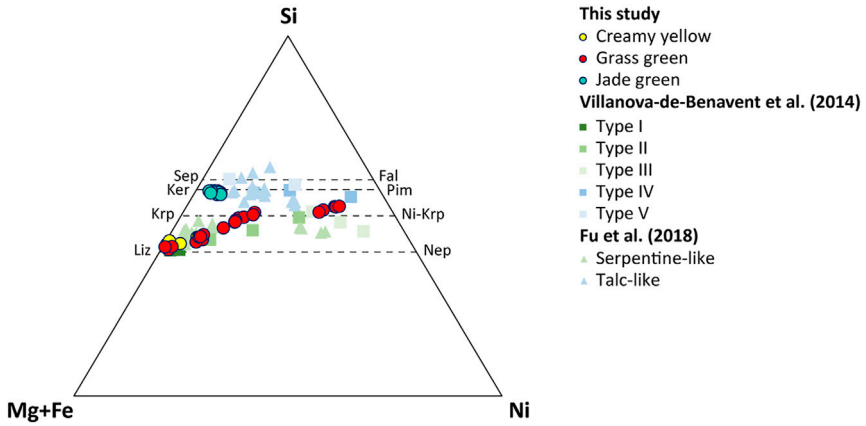

FIGURE 5 | Ternary diagram of Si-Mg + Fe-Ni system showing the garnierite phases in the Morowali deposit and other references. Abbreviation: Sep = sepiolite, Fal = falcondoite, Ker = kerolite, Pim = pimelite, Krp = karpinskite, Liz = lizardite, Nep = népouite.

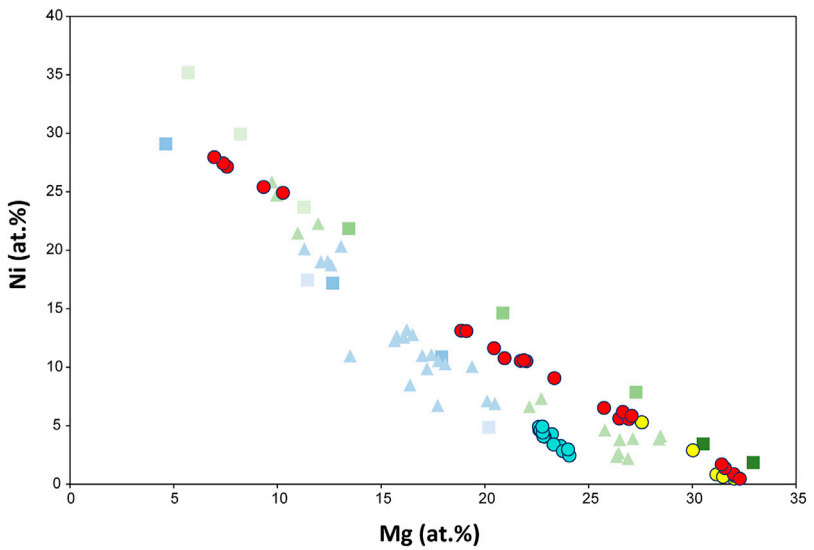

FIGURE 6 | Nickel content of garnierite samples from this study and other references as a function of Mg content in atomic percentage. Type I to V garnierites data are from Villanova-de-Benavent et al. (2014). Serpentine-like and talc-like garnierite data are from Fu et al. (2018). Legend is identical in **Figure 5**.

DISCUSSION

Nature of Garnierite in Morowali Deposit

Precipitation of Garnierite

The term garnierite has been widely used to denote a mixture of serpentine, talc, sepiolite, chlorite, and/or smectite phases due to its poor crystallinity, fine grain size, and ambiguous occurrences (Brindley and Hang, 1973; Springer, 1974). It is generally applied when mineral phases cannot be distinctly demarcated; however, the mineralogical term such as kerolite, which is an end member of the talc series, is sometimes used instead of garnierite when the occurrence of the mineral is known (Cathelineau et al., 2016). Nevertheless, based on the XRD results, where phases such as lizardite, chrysotile, talc, and sepiolite were observed but their origin was not known, we used the term garnierite to denote the Ni-rich phase.

The XRD results of the Morowali garnierite samples display two apparent end members, i.e., serpentine-like and talc-like phases. The creamy yellow and grass green garnierites show similar patterns, and are grouped under serpentine-like phase (**Figures 4A,B**). Even though the grass green garnierite patterns are more similar to the serpentine-like garnierite, some degree of similarity was also observed with the talc-like garnierite, which indicates that the grass green garnierite includes impurities of talc-like phases. These distinctive morphological features of each garnierite are also reflected in their chemical characteristics. Both creamy yellow and grass green serpentine-like garnierites plot between the lizardite-népouite and karpinskite-Ni-karpinskite

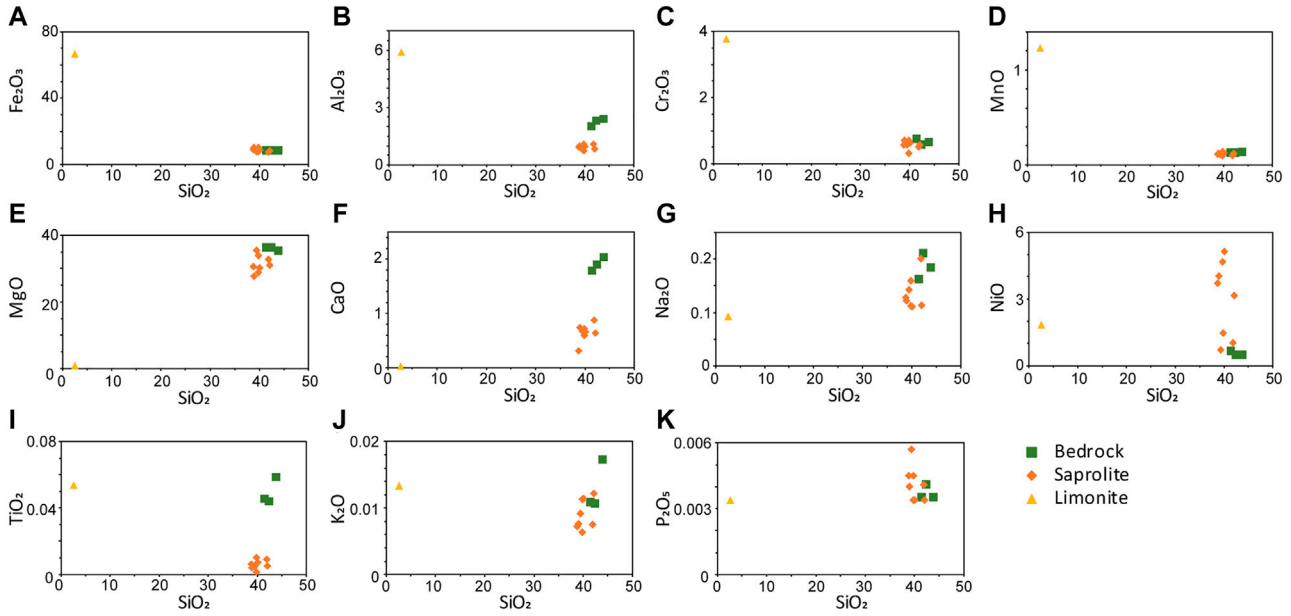

FIGURE 7 | Elemental distribution in bedrock, saprolite, and limonite horizons of the Morowali deposit. With the progress of laterization, a decrease in SiO_2 was observed.

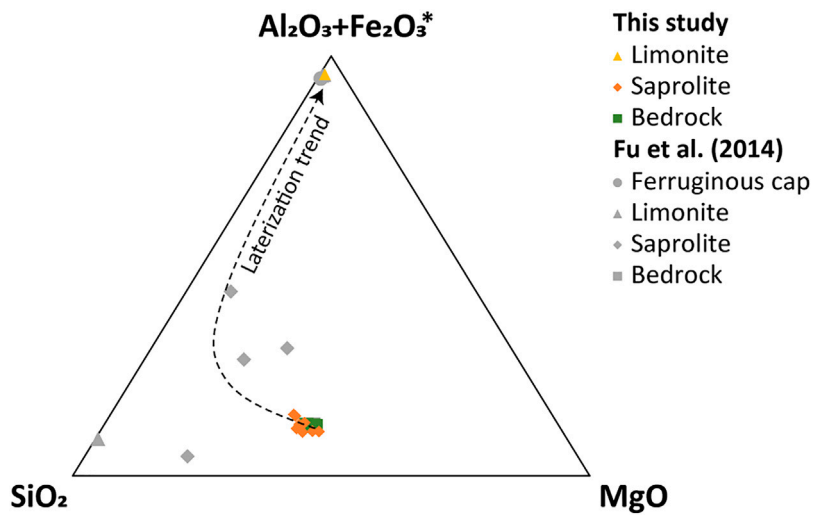

FIGURE 8 | Ternary diagram of Al_2O_3+Fe_2O_3*-SiO_2-MgO system for the laterite horizon in the Morowali deposit. Samples from this study are described in colored symbols and references from Indonesia (Fu et al., 2014) are represented by grey symbols. Fe_2O_3* means total iron oxide.

series (**Figure 5**). Lizardite and népouite are generally well-defined minerals, while karpinskite still lacks mineralogical validity (Fu et al., 2018). Karpinskite ideally maintains a T/O value of 1, and when it is present as an impurity in the serpentine- or talc-like phase, it might allow excess Si in the octahedral site (Tauler et al., 2009).

Three garnierite samples in the Morowali deposit show different physical and chemical characteristics suggesting that they originated from different sources. Iron content has been used as an indicator for determining the sequence of garnierite in many previous studies because of its immobile character during laterization (Villanova-de-Benavent et al., 2014; Fu et al., 2018). The creamy yellow serpentine-like garnierite (**Figure 5**) plots near lizardite and the FeO content (4.14–6.43 wt%) is analogous to that of serpentine in saprolite (4.14–7.41 wt%). This indicates that the creamy yellow garnierite originated from the surrounding serpentine. The grass green garnierite contains a wide range of FeO (0.14–7.03 wt%) and NiO (0.76–38.26 wt%) contents than the creamy yellow garnierite. The XRD pattern of the grass green garnierite exhibits the existence of talc phase

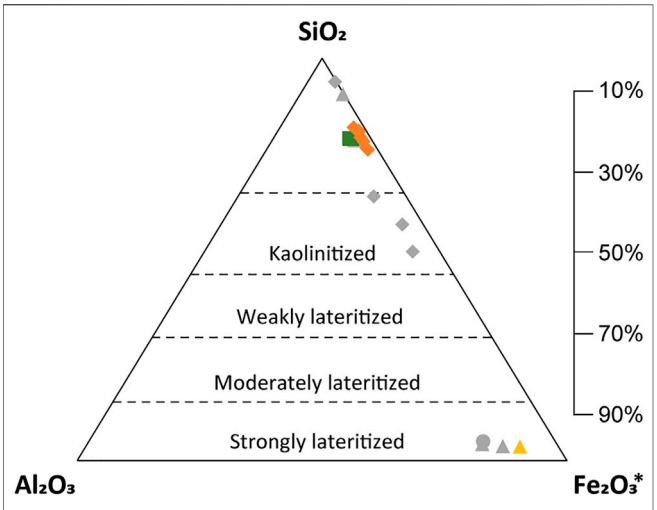

FIGURE 9 | Ternary diagram of SiO_2-Al_2O_3- Fe_2O_3* for the laterite horizon in the Morowali deposit and its index of lateritization (IOL). IOL represents the degree of weathering in the quantitative calculation of chemical composition. The calculation formula of IOL is as follows: IOL = $100x((Al_2O_3+Fe_2O_3*)/(SiO_2+Al_2O_3+Fe_2O_3*))$ (Tupaz et al., 2020). Legend is same as in **Figure 8**.

impurity. The NiO content is inversely proportional to the FeO and MgO contents, indicating active ion exchange between Mg and Ni. In addition, grass green garnierite occurs both as coating and as veinlet intruding the creamy yellow garnierite (**Figure 3G**) that covers the surface of the rocky saprolite as coatings. This means that both creamy yellow and grass green garnierites originated from the serpentine in saprolite by Mg-Ni exchange. However, the creamy yellow garnierite is more weathered and has a low Ni content than the grass green garnierite, which continues to interact with the Ni-rich solution passing through the saprolite horizon, precipitating Ni in the micro veins.

According to Manceau and Calas (1985), secondarily precipitated garnierite, which is neoformed garnierite from Ni-bearing solution, has a low iron content (<0.5 wt% FeO) because iron is insoluble during weathering. The iron content of the talc-like Morowali garnierites is < 0.05 wt% (FeO) (**Table 2**), indicating that their origin is secondary in nature. The talc-like garnierite not only shows a low Fe content but also a relatively low Ni content than the grass green serpentine-like garnierite. Their low Ni content suggests that the Ni in them comes from saprolite and not dierctly from the serpentine-like garnierites. Similar signatures were observed by Villanova-de-Benavent et al. (2014). Moreover, the oscillation texture in the talc-like garnierite (**Figure 3F**) indicates that precipitation of talc-like garnierite was accompanied by chemical changes (Fu et al., 2018).

Occurrence of Garnierite From Other Ni-Laterite Deposits

Garnierite occurring in the Morowali laterite can be divided into talc-like and serpentine-like. Such types of garnierites have also been reported from the Sorowako and Kolonodale deposits in Sulawesi (Sufriadin et al., 2011; Fu et al., 2018). These phases have also been discovered globally in New Caledonia (Manceau and Calas, 1985; Cluzel and Vigier, 2008; Wells et al., 2009), Dominican Republic (Proenza et al., 2008; Villanova-de-Benavent et al., 2014), Venezuela (Soler et al., 2008), and Colombia (Gleeson et al., 2004). The garnierite occurring in these countries shows a similar appearance, but their composition differs depending on the host rock and weathering environment. Therefore, for a comparative study, we selected garnierites that were formed in tropical climates and had bedrock compositions analogous to the Morowali samples (**Figures 5**, **6**). Villanova-de-Benavent et al. (2014) classified garnierites in the Falcondo Ni-laterite deposit, Dominican Republic, into five phases from type I to type V by using XRD and EPMA analyses. The Falcondo Ni-laterite deposit formed in a tropical climate and is hosted in partially serpentinized peridotite. It has the same climate conditions and host rock composition as that of the Morowali deposit. Similar to the study area, the Kolonodale deposit in Sulawesi, Indonesia is associated with the same ophiolite (East Sulawesi ophiolite), and has developed under the same climate conditions. The host rock of the Kolonodale deposit is regionally metamorphosed serpentinite (Fu et al., 2014; Fu et al., 2018). Garnierites from Kolonodale deposit are both serpentine- and talc-like.

The XRD patterns of the garnierites in the Morowali deposit show intensities similar to the patterns of the Falcondo deposit. The serpentine-like garnierite in this study corresponds to the type I, type II, and type III garnierite in Villanova-de-Benavent et al. (2014) while the talc-like garnierite from this study coincides with the type IV garnierite from Villanova-de-Benavent et al. (2014). Along with the XRD patterns, the chemical composition also indicates similarity between the Morowali and Falcondo deposits. The Ni and Mg contents (atomic percentage) of the studied garnierite samples (**Figure 6**) suggests that although the classification of Villanova-de-Benavent et al. (2014) is not absolute, garnierites in the Morowali deposit show similar development pathways as those of the Falcondo deposit. Contrastingly, garnierites from the Kolonodale deposit are more heterogeneous in composition than the Morowali deposit; for example, talc-like garnierites plot over serpentine-like garnierite in the Kolonodale deposit, indicating that along with the host rock composition as a primary factor in the formation of Ni-bearing laterite deposits, environmental influence also impacts the Ni enrichment in garnierite. The negative correlation between Mg and Ni implies that the process of garnierite formation is the same everywhere, i.e., by substitution of Mg by Ni. However, the Ni enrichment process in the serpentine- and talc-like phases is not completely understood yet.

Environment of the Morowali Ni-Laterite Deposit

Serpentinization-related extensive water–rock interaction might occur before laterization because most of the laterite deposits that develop on the bedrock are already serpentinized due to chemical reactions with seawater (Golightly, 1981). At low temperatures,

the primary minerals in peridotites, such as olivine and pyroxene, are altered faster than the hydrous phases, such as brucite, serpentine, and talc, because of their instability, and the alteration process continues until equilibrium is reached between the hydrous and primary minerals (Nesbitt and Bricker, 1978). Mesh-like textures are generally formed during serpentinization from seawater by the thermodynamically and kinetically controlled hydration processes (**Figure 3C, E-H**), and indicate olivine weathering (Viti and Mellini, 1998). Olivine hydration results in the formation of brucite and serpentine with minor magnetite (Tupaz et al., 2020). Magnetite formed during serpentinization develops at 200–300°C (Klein et al., 2014; Tupaz et al., 2020). The presence of magnetite associated with serpentine in the studied samples suggests that low-temperature hydration was the primary process that occurred before laterization.

Nickel laterite deposits are mostly developed on accretionary and cratonic terranes (Freyssinet et al., 2005; Butt and Cluzel, 2013). The study area (East Sulawesi ophiolite) is an accretionary terrane. Tectonic uplift plays an important role in the development of Ni-rich laterite profile since it forms faults and joints, which promote physical and chemical weathering along them (Cluzel and Vigier, 2008; Wells et al., 2009; Golightly, 2010; Butt and Cluzel, 2013; Furnes et al., 2014; Villanova-de-Benavent et al., 2014; Tauler et al., 2017). According to field observations, there is a thrust in the vicinity of the study area that uplifts the peridotite. The occurrence of garnierite, both as coatings and veins, along the joints and faults indicates that its precipitation was synchronous with the tectonic uplift. This process of garnierite precipitation is similar to the previous work on the supergene nickel deposit in New Caledonia (Cluzel and Vigier, 2008). Further, serpentine veins that crosscut the pre-existing serpentines and have a higher amount of Ni (**Figures 3D,H**) are a different type of serpentine that were probably formed after the bedrock was exposed to the surface (Tupaz et al., 2020). The occurrence of the crosscutting serpentine veins indicates that the bedrock was constantly weathered since its uplift. In addition, talc-like garnierite was not observed when the degree of weathering was low because the garnierite-forming solution did not become supersaturated (Tupaz et al., 2020b). This suggests that the Morowali Ni-laterite deposit is part of a good drainage system since it shows the presence of talc-like garnierite. The tropical weather of the study area supplies enough water, with an annual rainfall >1800 mm (Butt and Cluzel, 2013; Fu et al., 2014).

These mineralogical and textural characteristics of secondary alteration minerals, and uplifted tectonic setting indicate that the serpentinization had been occurred before uplift, and the uplift influenced the development of the Morowali Ni-laterite deposit.

Development of Laterite Profile

During laterization, water moves downward along the joints and fractures causing fluctuations in the water table, and leaches soluble elements from the host rock causing chemical reactions within the joints and fractures. The enrichment of immobile elements such as Fe, Al, Mn, Cr, and Ti in the limonite horizon is the result of weathering since as the water steadily moves downward, it leaves the immobile elements in the upper horizon (**Figures 7A–D,I**). The main dissolution reactions for element leaching can be explained by the equilibrium between mineral solubility and ion exchange (Golightly, 1981). Olivine dissolves first, followed by pyroxene, serpentine, talc, Ni-bearing minerals (nepouite and kerolite), gibbsite, and goethite (Golightly, 1981; Golightly, 2010). These mineral solubilities are controlled by pH, and increase as pH decreases, except for quartz (Golightly, 2010). Therefore, the degree of weathering can be inferred from the minerals in the horizon. Weathering of the primary minerals cause leaching of soluble alkaline elements (**Figures 7E,F**), and poorly crystalline Fe oxides, mostly goethite, and smectites are precipitated, which contain the Ni released from olivine and serpentine (Humphris and Thompson, 1978; Freyssinet et al., 2005). This observation is reflected in the relatively high NiO of the limonite horizon compared to the bedrock (**Figure 7H**). Alkaline elements prefer to remain in solution rather than precipitate as secondary minerals (Aiuppa et al., 2000), while the relatively immobile Fe and Al replace the element present in the dioctahedral site of smectite (Manceau and Calas, 1985). Continued weathering hydrolyzes the smectites, which causes the enrichment of Fe oxides with Al in the upper horizon (**Figure 8**). Repetition of this process increases porosity, which allows the solution to percolate easily (Freyssinet et al., 2005). This solution might be Ni-rich because during the reprecipitation of Fe oxides in the upper horizon, the Ni contained in goethite is released and incorporated in the garnierite-forming solution.

The garnierite-forming solution percolates downward until it reaches the depth where garnierite can be formed. Formation of garnierite is influenced by the pH; for example, a sudden change in pH from acidic to alkaline oversaturates the garnierite-forming solution causing garnierite precipitation (Golightly, 1979). In this process, Ni replaces Mg in the octahedral site of serpentine or other weathering products of the primary minerals because of their similar ionic radii, leading to Ni enrichment in the saprolite horizon.

The index of lateritization (IOL) was used to verify the degree of laterization (**Figure 9**). The IOL values divide the samples according to the degree of weathering (weak, moderate, and strong). The range of IOL values for the studied bedrock, saprolite, and limonite were 19.87–20.05, 17.18–22.7, and 96.57, respectively. The similar low IOL values of the bedrock and saprolite imply that the Morowali Ni laterite deposit underwent weak weathering in the saprolite horizon. In the Kolonodale deposit, the weathering of the saprolite horizon is also weakly weathered but more evolved than the Morowali deposit. However, high IOL values for the limonite horizon in the two deposits suggest that it is strongly weathered, leading to the formation of a thick limonite horizon and high Ni concentration in the saprolite horizon (Tupaz et al., 2020). In the Morowali Ni-laterite deposit, the saprolite and limonite horizons are 2–7 m thick, and the boundary between the two horizons is undulatory. In the Kolonodale deposit, the high Ni concentrated talc-like garnierite is observed (**Figure 6**), but some limonite is weakly weathered. Therefore, Ni concentration in the

saprolite horizon and the development of garnierite can differ depending on the location and degree of weathering.

Model of Morowali Ni-Laterite Deposit

Several generic evolution models have been proposed for laterite deposits (Golightly (1981); Freyssinet et al. (2005); Butt and Cluzel (2013). More specific models have been suggested based on these models. For example, Cathelineau et al. (2016) and Mongelli et al. (2019) insisted on the redistribution model for garnierite-forming elements in New Caledonia and Iran, respectively, while Fu et al. (2018) suggested a preferential flow model, in which preferential flow is the driving force for the Ni-rich solution. The redistribution model is that the pre-existing elements in the host rock are redistributed and formed nickel ore minerals according to changes in groundwater level or wet-dry season. The preferential flow model is that the precipitation of garnierite occurs mainly along preferential flow pathways, which are the pathways for water preferred to flow such as chemical and geological channels. The formation of the Morowali deposit corresponds to the prevalent models combined with the redistribution model.

Since its tectonic uplift in the Late Oligocene (Hall and Wilson, 2000), the serpentinized eastern Sulawesi ophiolite has undergone weathering because of the tropical climate of Indonesia due to large amount of precipitation, and the primary minerals in the bedrock have altered to smectite group minerals. In the process of laterization, immobile elements (Fe, Al, Mn, Cr, and Ti) remained in the upper horizons, and soluble elements (Mg and Si) were leached from the bedrock. The upper horizon has an oxidizing environment that results in the enrichment of redox-sensitive elements and the formation of Fe oxides (Robb, 2005). The Ni in olivine or serpentine is leached during weathering of the bedrock and reprecipitated in the Fe oxides, mostly goethite (Freyssinet et al., 2005).

As the dry and rainy seasons repeat, the water table fluctuates due to the meteoric water percolating into the bedrock that leads to redistribution of Ni preserved in goethite and formation of garnierite. The acidic meteoric water infiltrates the fractures and joints due to continued uplift. In this process, the Ni adsorbed in goethite, which is in the upper horizon, is leached and migrates downward with the solution (Freyssinet et al., 2005). The transported Ni reacts with the weathering products of ferromagnesian minerals by replacing Mg with Ni and finally producing a serpentine-like garnierite (Freyssinet et al., 2005; Butt, 2016). In the deeper horizon, the garnierite-forming solution percolates along the faults and joints and precipitates secondary talc-like garnierite with low FeO content (<0.5 wt% FeO), occurring as coatings between two blocks of serpentinized bedrock. According to Cathelineau et al. (2016), the talc-like garnierite-forming solution reaches the surface via vertical veins that were synchronous with faulting activity and joints, which contained early formed Ni-rich minerals, thus having high Ni content. However, the talc-like garnierite in this study had a low Ni content, suggesting that the talc-like garnierite-forming solution was a low-Ni-bearing fluid that originated in the saprolite horizon and precipitated garnierite from the outside of the horizontal vein. The garnierite and quartz mineralization occur in the dry season (Cathelineau et al., 2016; Mongelli et al., 2019).

However, the Ni-enriched vertical vein was not observed during the field investigation, which might be due to the frequent erosion of the laterite deposit during the rainy season. Cathelineau et al. (2016) found large Ni-bearing veins in their study area (New Caledonia) during open-pit mining, and they showed that changes in garnierite mineralization occurred within a few months. This means that large Ni-bearing veins can emerge from the Morowali deposit by continuing open-pit mining.

CONCLUSION

1) The Morowali Ni-laterite deposit in Indonesia is developed on the eastern Sulawesi ophiolite, and the host rock is mainly serpentinized harzburgite. The lateritic profile of the deposit is classified into three horizons: saprolite, limonite, and ferruginous cap from bottom to top. The boundaries of each horizon are irregular and undulatory. The main Ni ore is garnierite, which is a hydrous Mg-silicate, and is concentrated in the saprolite horizon. Garnierite is amorphous and exists as veins and coatings.
2) The studied garnierites can be chemically distinguished into serpentine- and talc-like. From the Fe (immobile) content, which is an indicator of the precipitation sequence of garnierite, it was inferred that the serpentine-like garnierite precipitated earlier than the talc-like garnierite. Both creamy yellow and grass green-colored varieties of serpentine-like garnierites originated from the surrounding serpentine. The creamy yellow garnierite was more weathered than the grass green garnierite. The low Ni concentration of talc-like garnierite suggest that they are secondary in nature, originating from saprolite and/or serpentine-like garnierite.
3) The laterite horizon in the Morowali deposit is formed by hydrous weathering. The weathered host rock shows a mesh-like texture resulting from olivine alteration and is composed of secondary minerals such as serpentine and clay minerals. These mineralogical changes caused the enrichment of immobile elements such as Fe, Al, Cr, Mn, and Ti in the limonite horizon, and soluble cations such as Mg are replaced by Ni in the saprolite horizon.
4) The Morowali Ni-laterite deposit is formed by the typical laterization and redistribution process. The tropical climate in the Morowali deposit is a driving force for the dissolution of Mg and Si during the rainy season and the precipitation of garnierite during the dry season. Since the uplift of the eastern Sulawesi ophiolite, chemical reactions occurred within the syntectonic faults and joints during laterization, and serpentine-like garnierite precipitated by replacing the Mg in lizardite with the Ni in solution. After syntectonic faults and joints were formed, meteoric water infiltrated along them to

form talc-like garnierite in the joints within the lower saprolite horizon.

DATA AVAILABILITY STATEMENT

The original contributions presented in the study are included in the article/supplementary material, further inquiries can be directed to the corresponding author.

AUTHOR CONTRIBUTIONS

YC, IL and IM carried out this study. All authors participated in field work. YC conducted analyses, and prepared manuscript and figures. IL and IM supervised all the process and gave advice on the manuscript. All authors reviewed the content of the work and agreed to be accountable for the manuscript.

FUNDING

This research is financially supported by projects 0409-20200243 and 0409-20210067 from National Research Foundation of Korea.

ACKNOWLEDGMENTS

We thank National Center for Inter-University Research Facility (NCIRF) for analyses, and the BK21 program from Seoul National University, Republic of Korea.

REFERENCES

Aiuppa, A., Allard, P., D'Alessandro, W., Michel, A., Parello, F., Treuil, M., et al. (2000). Mobility and Fluxes of Major, Minor and Trace Metals during basalt Weathering and Groundwater Transport at Mt. Etna Volcano (Sicily). *Geochimica et Cosmochimica Acta* 64 (11), 1827–1841. doi:10.1016/s0016-7037(00)00345-8

Barnes, S.-J., and Lightfoot, P. C. (2005). Formation of Magmatic Nickel-Sulfide Ore Deposits and Processses Affecting Their Copper and Platinum-Group Element Contents. *Econ. Geology*. 100th Anniversary volume, 179–213. doi:10.5382/av100.08

Brand, N. (1998). Nickel Laterites: Classification and Features. *AGSO J. Aust. Geol. Geophys.* 17, 81–88

Brindley, G. W., and Hang, P. T. (1973). The Nature of Garnierites-I Structures, Chemical Compositions and Color Characteristics. *Clays and Clay Minerals* 21 (1), 27–40. doi:10.1346/ccmn.1973.0210106

Brindley, G. W. (1980). The Structure and Chemistry of Hydrous Nickel-Containing Silicate and Nickel-Aluminium Hydroxy Minerals. *bulmi* 103 (2), 161–169. doi:10.3406/bulmi.1980.7391

Butt, C. R. M., and Cluzel, D. (2013). Nickel Laterite Ore Deposits: Weathered Serpentinites. *Elements* 9 (2), 123–128. doi:10.2113/gselements.9.2.123

Butt, C. R. M. (2016). The Development of Regolith Exploration Geochemistry in the Tropics and Sub-tropics. *Ore Geology. Rev.* 73, 380–393. doi:10.1016/j.oregeorev.2015.08.018

Cathelineau, M., Quesnel, B., Gautier, P., Boulvais, P., Couteau, C., and Drouillet, M. (2016). Nickel Dispersion and Enrichment at the Bottom of the Regolith: Formation of Pimelite Target-like Ores in Rock Block Joints (Koniambo Ni deposit, New Caledonia). *Miner Deposita* 51 (2), 271–282. doi:10.1007/s00126-015-0607-y

Cluzel, D., and Vigier, B. (2008). Syntectonic Mobility of Supergene Nickel Ores of New Caledonia (Southwest Pacific). Evidence from Garnierite Veins and Faulted Regolith. *Resource Geology.* 58 (2), 161–170. doi:10.1111/j.1751-3928.2008.00053.x

Dalvi, A. D,, Bacon, W. G., and Osborne, R. C. (2004). "The Past and the Future of Nickel Laterites," in *PDAC 2004 International Convention, Trade Show & Investors Exchange: Toronto: the Prospectors and Developers Association of Canada* (Ontario, Canada: Inco Limited), 1–27

Elias, M. (2002). "Nickel Laterite Deposits-Geological Overview, Resources and Exploitation," in *Giant Ore Deposits: Characteristics, Genesis and Exploration* (Chania, Crete, Greece: CODES Special Publication), 4, 205–220

Freyssinet, P., Butt, C., Morris, R., and Piantone, P. (2005). Ore-forming Processes Related to Lateritic Weathering. *Econ. Geology*. 100th Anniversary volume, 681–722. doi:10.5382/av100.21

Fu, W., Yang, J., Yang, M., Pang, B., Liu, X., Niu, H., et al. (2014). Mineralogical and Geochemical Characteristics of a Serpentinite-Derived Laterite Profile from East Sulawesi, Indonesia: Implications for the Lateritization Process and Ni Supergene Enrichment in the Tropical Rainforest. *J. Asian Earth Sci.* 93, 74–88. doi:10.1016/j.jseaes.2014.06.030

Fu, W., Zhang, Y., Pang, C., Zeng, X., Huang, X., Yang, M., et al. (2018). Garnierite Mineralization from a Serpentinite-Derived Lateritic Regolith, Sulawesi Island, Indonesia: Mineralogy, Geochemistry and Link to Hydrologic Flow Regime. *J. Geochemical Exploration* 188, 240–256. doi:10.1016/j.gexplo.2018.01.022

Furnes, H., De Wit, M., and Dilek, Y. (2014). Four Billion Years of Ophiolites Reveal Secular Trends in Oceanic Crust Formation. *Geosci. Front.* 5 (4), 571–603. doi:10.1016/j.gsf.2014.02.002

Gleeson, S. A., Herrington, R. J., Durango, J., Velásquez, C. A., and Koll, G. (2004). The Mineralogy and Geochemistry of the Cerro Matoso S.A. Ni Laterite Deposit, Montelibano, Colombia. *Econ. Geology.* 99 (6), 1197–1213. doi:10.2113/gsecongeo.99.6.1197

Golightly, J. (1981). Nickeliferous Laterite Deposits. *Econ. Geology. 75th Anniversary* 1905-1980, 710–734. doi:10.5382/av75.18

Golightly, J. (1979). "Nickeliferous Laterites: A General Description," in *International Laterite Symposium Proceedings* (New Orleans: Society of Mining Engineers, American Institute of Mining, Metallurgical, and Petroleum Engineers), 38–56

Golightly, J. (2010). Progress in Understanding the Evolution of Nickel Laterites. *The Challenge Finding New Mineral. Resources: Glob. Metallogeny, Innovative Exploration, New Discoveries* 2, 451–475. doi:10.5382/sp.15.2.07

Hall, R. (1997). Cenozoic Plate Tectonic Reconstructions of SE Asia. *Geol. Soc. Lond. Spec. Publications* 126 (1), 11–23. doi:10.1144/gsl.sp.1997.126.01.03

Hall, R., and Wilson, M. E. J. (2000). Neogene Sutures in Eastern Indonesia. *J. Asian Earth Sci.* 18 (6), 781–808. doi:10.1016/s1367-9120(00)00040-7

Humphris, S. E., and Thompson, G. (1978). Trace Element Mobility during Hydrothermal Alteration of Oceanic Basalts. *Geochimica et cosmochimica acta* 42 (1), 127–136. doi:10.1016/0016-7037(78)90222-3

Kadarusman, A., Miyashita, S., Maruyama, S., Parkinson, C. D., and Ishikawa, A. (2004). Petrology, Geochemistry and Paleogeographic Reconstruction of the East Sulawesi Ophiolite, Indonesia. *Tectonophysics* 392 (1-4), 55–83. doi:10.1016/j.tecto.2004.04.008

Katili, J. A. (1978). Past and Present Geotectonic Position of Sulawesi, Indonesia. *Tectonophysics* 45 (4), 289–322. doi:10.1016/0040-1951(78)90166-x

Klein, F., Bach, W., Humphris, S. E., Kahl, W.-A., Jöns, N., Moskowitz, B., et al. (2014). Magnetite in Seafloor Serpentinite--Some like it Hot. *Geology* 42 (2), 135–138. doi:10.1130/g35068.1

Manceau, A., and Calas, G. (1985). Heterogeneous Distribution of Nickel in Hydrous Silicates from New Caledonia Ore Deposits. *Am. Mineral.* 70 (5-6), 549–558

Mongelli, G., Taghipour, B., Sinisi, R., and Khadivar, S. (2019). Mineralization and Element Redistribution in the Chah-Gheib Ni-Laterite Ore Zone, Bavanat, Zagros Belt, Iran. *Ore Geology. Rev.* 111. 102990. doi:10.1016/j.oregeorev.2019.102990

Monnier, C., Girardeau, J., Maury, R. C., and Cotten, J. (1995). Back-arc basin Origin for the East Sulawesi Ophiolite (Eastern Indonesia). *Geol* 23 (9), 851–854. doi:10.1130/0091-7613(1995)023<0851:baboft>2.3.co;2

Mudd, G. M. (2010). Global Trends and Environmental Issues in Nickel Mining: Sulfides versus Laterites. *Ore Geology. Rev.* 38 (1-2), 9–26. doi:10.1016/j.oregeorev.2010.05.003

Mudd, G. M., and Jowitt, S. M. (2014). A Detailed Assessment of Global Nickel Resource Trends and Endowments. *Econ. Geology.* 109 (7), 1813–1841. doi:10.2113/econgeo.109.7.1813

Nesbitt, H. W., and Bricker, O. P. (1978). Low Temperature Alteration Processes Affecting Ultramafic Bodies. *Geochimica et Cosmochimica Acta* 42 (4), 403–409. doi:10.1016/0016-7037(78)90271-5

Parkinson, C. (1998). Emplacement of the East Sulawesi Ophiolite: Evidence from Subophiolite Metamorphic Rocks. *J. Asian Earth Sci.* 16 (1), 13–28. doi:10.1016/s0743-9547(97)00039-1

Proenza, J. A., Lewis, J. F., Galí, S., Tauler, E., Labrador, M., Melgarejo, J., et al. (2008). Garnierite Mineralization from Falcondo Ni-Laterite deposit (Dominican Republic). *Macla* 9, 197–198

Robb, L. J. (2005). *Introduction to Ore-Forming Processes*. United States: Blackwell Publishing

Soler, J. M., Cama, J., Gali, S., Meléndez, W., Ramírez, A., and Estanga, J. (2008). Composition and dissolution kinetics of garnierite from the Loma de Hierro Ni-laterite deposit, Venezuela. *Chem. Geology.* 249 (1-2), 191–202. doi:10.1016/j.chemgeo.2007.12.012

Springer, G. (1974). Compositional and Structural Variations in Garnierites. *Can. Mineral.* 12 (6), 381–388

Stevens, C., McCaffrey, R., Bock, Y., Genrich, J., Endang, C., Subarya, C., et al. (1999). Rapid Rotations about a Vertical axis in a Collisional Setting Revealed by the Palu Fault, Sulawesi, Indonesia. *Geophys. Res. Lett.* 26 (17), 2677–2680. doi:10.1029/1999gl008344

Sufriadin, S., Idrus, A., Pramumijoyo, S., Warmada, I. W., and Imai, A. (2011). Study on Mineralogy and Chemistry of the Saprolitic Nickel Ores from Soroako, Sulawesi, Indonesia: Implication for the Lateritic Ore Processing. *J. Appl. Geology.* 3 (1), 23–33. doi:10.22146/jag.7178

Tauler, E., Lewis, J. F., Villanova-de-Benavent, C., Aiglsperger, T., Proenza, J. A., Domènech, C., et al. (2017). Discovery of Ni-Smectite-Rich Saprolite at Loma Ortega, Falcondo Mining District (Dominican Republic): Geochemistry and Mineralogy of an Unusual Case of "hybrid Hydrous Mg Silicate - clay Silicate" Type Ni-Laterite. *Miner Deposita* 52 (7), 1011–1030. doi:10.1007/s00126-017-0750-8

Tauler, E., Proenza, J. A., Galí, S., Lewis, J. F., Labrador, M., García-Romero, E., et al. (2009). Ni-sepiolite-falcondoite in Garnierite Mineralization from the Falcondo Ni-Laterite deposit, Dominican Republic. *Clay miner.* 44 (4), 435–454. doi:10.1180/claymin.2009.044.4.435

Tupaz, C. A. J., Watanabe, Y., Sanematsu, K., Echigo, T., Arcilla, C., and Ferrer, C. (2020). Ni-Co Mineralization in the Intex Laterite Deposit, Mindoro, Philippines. *Minerals* 10 (7), 579. doi:10.3390/min10070579

Van der Ent, A., Baker, A. J. M., Van Balgooy, M. M. J., and Tjoa, A. (2013). Ultramafic Nickel Laterites in Indonesia (Sulawesi, Halmahera): Mining, Nickel Hyperaccumulators and Opportunities for Phytomining. *J. Geochemical Exploration* 128, 72–79. doi:10.1016/j.gexplo.2013.01.009

Villanova-de-Benavent, C., Proenza, J. A., Galí, S., García-Casco, A., Tauler, E., Lewis, J. F., et al. (2014). Garnierites and Garnierites: Textures, Mineralogy and Geochemistry of Garnierites in the Falcondo Ni-Laterite deposit, Dominican Republic. *Ore Geology. Rev.* 58, 91–109. doi:10.1016/j.oregeorev.2013.10.008

Viti, C., and Mellini, M. (1998). Mesh Textures and Bastites in the Elba Retrograde Serpentinites. *ejm* 10 (6), 1341–1360. doi:10.1127/ejm/10/6/1341

Wells, M. A., Ramanaidou, E. R., Verrall, M., and Tessarolo, C. (2009). Mineralogy and crystal Chemistry of "Garnierites" in the Goro Lateritic Nickel deposit, New Caledonia. *ejm* 21 (2), 467–483. doi:10.1127/0935-1221/2009/0021-1910

Wilson, M. E. J., and Moss, S. J. (1999). Cenozoic Palaeogeographic Evolution of Sulawesi and Borneo. *Palaeogeogr. Palaeoclimatol. Palaeoecol.* 145 (4), 303–337. doi:10.1016/s0031-0182(98)00127-8

Conflict of Interest: The authors declare that the research was conducted in the absence of any commercial or financial relationships that could be construed as a potential conflict of interest.

Publisher's Note: All claims expressed in this article are solely those of the authors and do not necessarily represent those of their affiliated organizations, or those of the publisher, the editors and the reviewers. Any product that may be evaluated in this article, or claim that may be made by its manufacturer, is not guaranteed or endorsed by the publisher.